Article

# Tungsten Allylimido Complexes Cl(RCN)W(NCH) as Single-Source CVD Precursors for WNC Thin Films. Correlation of Precursor Fragmentation to Film Properties

Omar J. Bchir, Kelly M. Green, Hiral M. Ajmera, Elizabeth A. Zapp, Timothy J. Anderson, Benjamin C. Brooks, Laurel L. Reitfort, David H. Powell, Khalil A. Abboud, and Lisa McElwee-White

*J. Am. Chem. Soc.*, **2005**, 127 (21), 7825-7833• DOI: 10.1021/ja043799d • Publication Date (Web): 06 May 2005



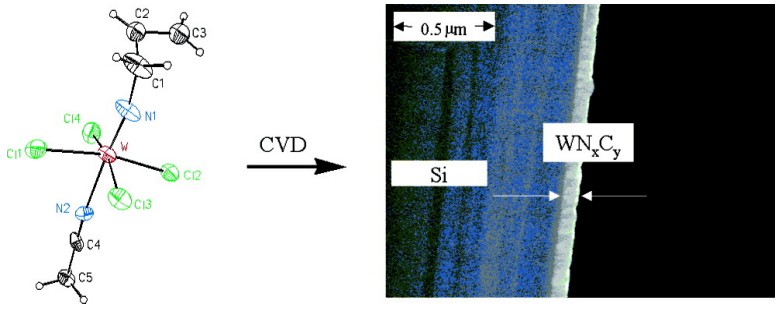


## More About This Article

Additional resources and features associated with this article are available within the HTML version:

- Supporting Information
- Links to the 4 articles that cite this article, as of the time of this article download
- Access to high resolution figures
- Links to articles and content related to this article
- Copyright permission to reproduce figures and/or text from this article

View the Full Text HTML

J|A|C|S
ARTICLES
Published on Web 05/06/2005

# Tungsten Allylimido Complexes $Cl_4(RCN)W(NC_3H_5)$ as Single-Source CVD Precursors for $WN_xC_y$ Thin Films. Correlation of Precursor Fragmentation to Film Properties

Omar J. Bchir,[†] Kelly M. Green,[†] Hiral M. Ajmera,[†] Elizabeth A. Zapp,[†] Timothy J. Anderson,*[,†] Benjamin C. Brooks,[‡,§] Laurel L. Reitfort,[‡] David H. Powell,[‡] Khalil A. Abboud,[‡] and Lisa McElwee-White*[,‡]

*Contribution from the Departments of Chemistry and Chemical Engineering, University of Florida, Gainesville, Florida 32611*

Received October 11, 2004; E-mail: tim@ufl.edu; lmwhite@chem.ufl.edu.

***Abstract:*** A mixture of the tungsten allylimido complexes $Cl_4(RCN)W(NC_3H_5)$ (**3a**, R = $CH_3$ and **3b**, R = Ph) was tested as a single-source precursor for growth of tungsten nitride ($WN_x$) or carbonitride ($WN_xC_y$) thin films. Films deposited from **3a**,**b** below 550 °C contained amorphous $\beta$-$WN_xC_y$, while those deposited at higher temperatures were polycrystalline. Film growth rates from **3a**,**b** ranged from 5 to 10 Å/min over a temperature range of 450−650 °C, and the apparent activation energy for film growth was 0.15 eV. A plot of the $E_a$ values for deposition from $Cl_4(RCN)W(NR')$ [R′ = Ph, $^i$Pr, allyl] against the N−C imido bond strengths for the analogous amines $R'NH_2$ is linear, implicating cleavage of the N−C bond as the rate-determining step in film growth. The correlation of mass spectral fragmentation patterns for $Cl_4(RCN)W(NR')$ with film properties such as nitrogen content supports the significance of facile N−C bond cleavage in film growth.

## Introduction

As feature sizes on integrated circuits (ICs) continue to decrease with successive device generations, the layer thickness of many materials on the device also decreases. A major challenge for the semiconductor industry is to develop effective routes to deposit thin diffusion barrier layers, which prevent Cu from diffusing into neighboring layers on the circuit. The barrier layer must conformally coat small diameter, high aspect ratio features and must effectively prevent Cu diffusion at successively decreasing barrier thicknesses. The ideal diffusion barrier material should also have low resistivity, amorphous microstructure, and low deposition temperatures (<400 °C).

Thin films of refractory metal nitrides are among the most promising materials being considered for barrier applications in copper-containing ICs.[1] Excess nitrogen present in these materials can migrate to grain boundaries, helping to block these potential diffusion pathways through repulsive Cu−N interactions.[2,3] An example of a refractory metal nitride that has found applications in IC technology is tantalum nitride (TaN), which has been used as a barrier material for intermediate and upper level wiring in some IC devices.[4] Another metal nitride that is a promising candidate for thin film barrier materials is tungsten nitride ($WN_x$).[5−7] This material has the additional advantages of increased adhesion to copper,[8] potential seedless copper electrodeposition,[9−11] and facile processing (e.g., more efficient chemical mechanical polishing).[12] In addition to these binary nitrides, the ternary material tungsten carbonitride ($WN_xC_y$) has also shown promise for diffusion barrier applications. This material is reported to have low resistivity, good adhesion to Cu, and effective resistance to Cu diffusion following annealing to 700 °C.[13−15]

Chemical vapor deposition (CVD) is a useful technique for growth of thin films for barrier material applications. In this process, the material is deposited on the substrate by reaction of one (i.e., single-source) or more (i.e., co-reactant) precursor molecules. Previous examples of $WN_x$ deposited by CVD

[†] Department of Chemical Engineering.
[‡] Department of Chemistry.
[§] Current address: Department of Natural Sciences, Gardner-Webb University, Boiling Springs, NC 28017.

(1) Nicolet, M. A.; Bartur, M. *J. Vac. Sci. Technol.* **1981**, *19*, 786−793.
(2) Ekstrom, B. M.; Lee, S.; Magtoto, N.; Kelber, J. A. *Appl. Surf. Sci.* **2001**, *171*, 275−282.
(3) Shamir, N.; Lin, J. C.; Gomer, R. *Surf. Sci.* **1989**, *214*, 74−84.
(4) Winter, C. H. *Aldrichim. Acta* **2000**, *33*, 3−12.
(5) Ganguli, S.; Chen, L.; Levine, T.; Zheng, B.; Chang, M. *J. Vac. Sci. Technol., B* **2000**, *18*, 237−241.
(6) Li, H.; Jin, S.; Bender, H.; Lanckmans, F.; Heyvaert, I.; Maex, K.; Froyen, L. *J. Vac. Sci. Technol., B* **2000**, *18*, 242−251.
(7) Pokela, P. J.; Kwok, C. K.; Kolawa, E.; Raud, S.; Nicolet, M. A. *Appl. Surf. Sci.* **1991**, *53*, 364−372.
(8) Ivanova, A. R.; Galewski, C. J.; Sans, C. A.; Seidel, T. E.; Grunow, S.; Kumar, K.; Kaloyeros, A. E. *Mater. Res. Soc. Symp. Proc.* **1999**, *564*, 321−326.
(9) Singer, P. *Semiconductor International*; Reed-Elsevier: 2002; Vol. 25, pp 46−53.
(10) Shaw, M. J.; Grunow, S.; Duquette, D. J. *J. Electron. Mater.* **2001**, *30*, 1602−1608.
(11) *International Technology Road map for Semiconductors*, 2001 ed.; International SEMATECH: Austin, TX, 1999.
(12) Galewski, C.; Seidel, T. *Eur. Semiconductor* **1999**, 31−32.
(13) Kim, S.-H.; Oh, S. S.; Kim, K.-B.; Kang, D.-H.; Li, W.-M.; Haukka, S.; Tuominen, M. *Appl. Phys. Lett.* **2003**, *82*, 4486−4488.
(14) Li, W.-M.; Tuominen, M.; Haukka, S.; Sprey, H.; Raaijmakers, I. J. *Solid State Technol.* **2003**, *46*, 103−104, 106.
(15) Kim, S.-H.; Oh, S. S.; Kim, H.-M.; Kang, D.-H.; Kim, K.-B.; Li, W.-M.; Haukka, S.; Tuominen, M. *J. Electrochem. Soc.* **2004**, *151*, C272−C282.

include co-reactant systems utilizing $WF_6$, $WCl_6$, and $WO_3$ as the tungsten source and $NH_3$ as the nitrogen source.[16−21] Similarly, organometallic co-reactant precursors such as $W(CO)_6$ and $W(CO)_5(C_5H_{11}NC)$ have also been employed with $NH_3$.[22,23] Apart from recent examples from our laboratory, the only example of a single-source $WN_x$ precursor is the bis(imido) bis(amido) tungsten complex $(^tBuNH)_2W(N^tBu)_2$.[24,25] Interestingly, use of the related precursor $(Me_2N)_2W(N^tBu)_2$ with $NH_3$ in atomic layer deposition (ALD) experiments has also been reported.[26,27] Ternary $WN_xC_y$ films have been deposited by ALD, most often using sequential reactions of $WF_6$, $NH_3$, and $B(C_2H_5)_3$.[13−15]

Previously, we have reported two other single-source precursors for $WN_x/WN_xC_y$ deposition, $Cl_4(RCN)W(N^iPr)$ (**1a**, R = $CH_3$ and **1b**, R = Ph)[28,29] and $Cl_4(RCN)W(NPh)$ (**2a**, R = $CH_3$ and **2b**, R = Ph).[30] Our interest in imido complexes arises from the fact that the strong W−N multiple bond of the precursor is likely to survive the deposition process and facilitate incorporation of nitrogen into the film. Additionally, the linear geometry of the triple bond directs the alkyl or aromatic group of the imido ligand away from the metal, thus deterring any cyclometalation process. Moreover, by changing this group, the N−C homolytic bond strength of the imido moiety is tunable, which should allow for a degree of control over film composition and other characteristics.

We have demonstrated that the isopropylimido precursor **1a**,**b** affords increased N incorporation relative to the phenylimido precursor **2a**,**b**, presumably due to the weaker N−C imido bond of the former.[28−31] Moreover, results for growth from **1a**,**b** and **2a**,**b** indicate a direct relationship between the strength of the N−C imido bond and the apparent activation energy for film growth in the kinetically limited regime. Thus, we reasoned that a more promising precursor would contain a weaker N−C imido bond than precursors **1a**,**b** or **2a**,**b**. Herein, we report the mass spectral data, solid-state structural characteristics, and film properties observed for deposition of films from the allylimido precursors $Cl_4(RCN)W(NC_3H_5)$ (**3a**, R = $CH_3$ and **3b**, R = Ph) as well as comparison of these properties with those of films deposited from **1a**,**b** and **2a**,**b**.

## Experimental Procedures

**General (Precursor Synthesis).** Standard Schlenk and glovebox techniques were employed in the synthesis of $Cl_4(CH_3CN)W(NC_3H_5)$ (**3a**). Allyl isocyanate was purchased from Aldrich and used without further purification. Anhydrous heptane was purchased from Aldrich in a Sure-Seal bottle and used as received. All other solvents were purchased from Fisher and passed through an M. Braun MB-SP solvent purification system prior to use. Tungsten oxychloride was prepared by a slightly modified literature method.[32] The benzonitrile complex $Cl_4(PhCN)W(NC_3H_5)$ (**3b**) was not isolated but was produced in situ by the substitution of the acetonitrile ligand of **3a** with benzonitrile, which was utilized as the solvent for the deposition experiments (vide infra). NMR solvents were degassed by three freeze−pump−thaw cycles and stored over 3 Å molecular sieves in an inert atmosphere glovebox. $^1H$ and $^{13}C$ NMR spectra were recorded on VXR 300 or Inova 500 spectrometers. In cases where assignments of $^1H$ or $^{13}C$ NMR resonances were ambiguous, $^{13}C-^1H$ HMQC experiments were used. Elemental analyses were performed by Robertson Microlit (Madison, NJ).

**$Cl_4(CH_3CN)W(NC_3H_5)$ (3a).** In a glovebox, tungsten oxychloride (1.229 g, 3.597 mmol) was slurried in a solution of allyl isocyanate (0.366 g, 4.41 mmol) in heptane (60 mL) in a sealed Chemglass 350 mL heavy wall pressure vessel with a Teflon bushing. The vessel was removed from the glovebox, and the mixture was heated for 36 h at 110 °C. The solvent was removed from the resulting dark red solution on a vacuum line. The reddish brown residue was dissolved in a minimal amount of $CH_3CN$ (approximately 10 mL). The resulting solution was stirred for 2 h, and the solvent was removed under reduced pressure. The resulting brown residue was washed with 5 × 10 mL of toluene, and the extracts were concentrated to approximately 5 mL. Hexane was added to precipitate the product. The orange−brown solid was filtered and washed with hexane to afford 0.974 g (64% yield) of the imido complex. $^1H$ NMR ($CDCl_3$) $\delta$ 7.55 (ddd, $J$ = 1.5, 1.4, 5.6 Hz, 2H, $NCH_2CHCH_2$); 6.07 (tdd, $J$ = 5.6, 10.2, 17.1 Hz, 1H, $NCH_2CHCH_2$); 5.73 (dtd, $J$ = 0.6, 1.5, 17.1 Hz, 1H, $NCH_2CHCH_2$); 5.60 (dtd, $J$ = 0.6, 1.4, 10.2 Hz, 1H, $NCH_2CHCH_2$); 2.50 (s, 3H, $CH_3CN$). $^{13}C$ NMR ($CDCl_3$, $\delta$): 129.7 ($CH_2CHCH_2N$); 121.9 ($CH_2CHCH_2N$); 118.9 ($CH_3CN$); 68.3 ($CH_2CHCH_2N$); 3.5 ($CH_3CN$). IR (KBr) 2929, 2314, 2287, 1649, 1409, 1364, 1317, 989, 919 $cm^{-1}$. mp 148−152 °C (dec). Anal. Calcd for $C_5H_8N_2Cl_4W$: C, 14.24%, H, 1.91%, N, 6.64%. Found: C, 14.51%, H, 1.86%, N, 6.43%.

**Mass Spectrometry.** All mass spectral analyses were performed using a Finnigan MAT95Q hybrid sector mass spectrometer (Thermo Finnigan, San Jose, CA). Electron ionization (EI) was carried out in positive ion mode using electrons of 70 eV potential and a source temperature of 200 °C. Negative ion electron capture chemical ionization (NCI) used methane as the bath gas at an indicate pressure of $2 \times 10^{-5}$ Torr, an electron energy of 100 V, and a source temperature of 120 °C. All samples were introduced via a controlled temperature probe with heating and cooling enabling temperature control down to 35 °C. The mass resolving power ($m/\Delta m$) was 5000 full width-half-maximum (fwhm).

**Crystallographic Structural Determination of 3a.** Data were collected at 173 K on a Siemens SMART PLATFORM equipped with a CCD area detector and a graphite monochromator utilizing MoK$\alpha$ radiation ($\lambda$ = 0.71073 Å). Cell parameters were refined using up to 8192 reflections. A full sphere of data (1850 frames) was collected using the $\omega$-scan method (0.3° frame width). The first 50 frames were remeasured at the end of data collection to monitor instrument and crystal stability (maximum correction on $I$ was < 1%). Absorption corrections by integration were applied based on measured indexed crystal faces.

The structure was solved by the Direct Methods in SHELXTL6[33] and refined using full-matrix least squares. The non-H atoms were

(16) Marcus, S. D.; Foster, R. F. *Thin Solid Films* **1993**, *236*, 330−333.
(17) Nagai, M.; Kishida, K. *Appl. Surf. Sci.* **1993**, *70−1*, 759−762.
(18) Lee, C. W.; Kim, Y. T.; Lee, C.; Lee, J. Y.; Min, S. K.; Park, Y. W. *J. Vac. Sci. Technol., B* **1994**, *12*, 69−72.
(19) Lee, C. W.; Kim, Y. T.; Min, S. K. *Appl. Phys. Lett.* **1993**, *62*, 3312−3314.
(20) Nakajima, T.; Watanabe, K.; Watanabe, N. *J. Electrochem. Soc.* **1987**, *134*, 3175−3178.
(21) Iguchi, K.; Urai, M.; Shiga, C.; Koba, M. Manufacture of Integrated Circuits. JP Patent 01005015, 1989.
(22) Kelsey, J. E.; Goldberg, C.; Nuesca, G.; Peterson, G.; Kaloyeros, A. E.; Arkles, B. *J. Vac. Sci. Technol., B* **1999**, *17*, 1101−1104.
(23) Gordon, R. G.; Barry, S.; Broomhall-Dillard, R. N. R.; Wagner, V. A.; Wang, Y. *Mater. Res. Soc. Symp. Proc.* **2000**, *612*, D9.12/11−D19.12/16.
(24) Chiu, H. T.; Chuang, S. H. *J. Mater. Res.* **1993**, *8*, 1353−1360.
(25) Tsai, M. H.; Sun, S. C.; Chiu, H. T.; Chuang, S. H. *Appl. Phys. Lett.* **1996**, *68*, 1412−1414.
(26) Becker, J. S.; Gordon, R. G. *Appl. Phys. Lett.* **2003**, *82*, 2239−2241.
(27) Becker, J. S.; Suh, S.; Wang, S.; Gordon, R. G. *Chem. Mater.* **2003**, *15*, 2969−2976.
(28) Bchir, O. J.; Johnston, S. W.; Cuadra, A. C.; Anderson, T. J.; Ortiz, C. G.; Brooks, B. C.; Powell, D. H.; McElwee-White, L. *J. Cryst. Growth* **2003**, *249*, 262−274.
(29) Bchir, O. J.; Anderson, T. J.; Brooks, B. C.; McElwee-White, L. In *Chemical Vapor Deposition: CVD XVI (16th)*; Allendorf, M., Maury, F., Teyssandier, F., Eds.; Electrochemical Society: Pennington, NJ, 2003; Vol. 2003-08, pp 424−431.
(30) Bchir, O. J.; Green, K. M.; Hlad, M. S.; Anderson, T. J.; Brooks, B. C.; Wilder, C. B.; Powell, D. H.; McElwee-White, L. *J. Organomet. Chem.* **2003**, *684*, 338−350.
(31) Bchir, O. J.; Green, K. M.; Hlad, M. S.; Anderson, T. J.; Brooks, B. C.; McElwee-White, L. *J. Cryst. Growth* **2004**, *261*, 280−288.
(32) Pedersen, S. F.; Schrock, R. R. *J. Am. Chem. Soc.* **1982**, *104*, 7483−7491.
(33) *SHELXTL6*; Bruker-AXS: Madison, WI, 2000.

***Table 1.*** Summary of Relative Abundances for Positive Ion EI and Negative Ion NCI Mass Spectra of Tungsten Imido Complexes $Cl_4(CH_3CN)W(NC_3H_5)$ (**3a**)

| EI fragments | NCI fragments | *m*/*z* | abundance[a] |
|---|---|---|---|
| $[Cl_3W(NC_3H_5)]^+$ | | 346 | 100 |
| $[Cl_4W]^+$ | | 326 | 34 |
| $[Cl_3WNH]^+$ | | 306 | 12 |
| $[Cl_3W]^+$ | | 291 | 58 |
| $[Cl_2W]^+$ | | 256 | 27 |
| $[CH_3CN]^+$ or $[C_3H_5]^+$ | | 41 | 95 |
| | $[Cl_4W(NC_3H_5)]^-$ | 381 | 5 |
| | $[Cl_4WN]^-$ | 340 | 100 |

[a] Relative abundances were adjusted by summing the observed intensities for the predicted peaks of each mass envelope and normalizing the largest sum to 100%.

treated anisotropically, whereas the hydrogen atoms were calculated in ideal positions and were riding on their respective carbon atoms. The C2−C3 moiety is disordered and was refined in two parts (the other part being C2′−C3′ with their site occupation factors dependently refined). Atom C1 is apparently also disordered but to a lesser extent than the C2−C3 moiety. It could not be resolved and was refined in the final model as not disordered. Refinement was done using $F^2$.

**Film Growth Studies.** The solid precursor **3a** was dissolved in benzonitrile at a concentration of 7.5 mg/mL, loaded into a syringe, and pumped into a nebulizer. Operation of the nebulizer was described previously.[28] Experiments were conducted in a custom-built vertical quartz cold wall CVD reactor system. *P*-type boron doped Si (100) substrates with resistivity of 1−2 Ω cm were used for the film growths. Growths were conducted for a fixed time period of 150 min at temperatures ranging from 425 to 675 °C. The system was maintained at vacuum by a mechanical roughing pump, with the operating pressure fixed at 350 Torr. Hydrogen ($H_2$) carrier gas was used for the depositions.

Film structure was examined by X-ray diffraction (XRD) on a Philips APD 3720, operating from 5 to 85 $2\theta$ degrees with CuKα radiation. Film composition was determined by Auger electron spectroscopy (AES) using a Perkin-Elmer PHI 660 Scanning Auger Multiprobe, while film sheet resistance was measured with an Alessi Industries four-point probe. Film thickness was estimated by cross-sectional scanning electron microscopy (X-SEM) on a JEOL JSM-6400, with growth rate calculated by dividing film thickness by deposition time.

## Results and Discussion

**Mass Spectrometry.** Correlation between the mass spectrometric fragmentation patterns of precursors and likely decomposition pathways during CVD has been previously postulated in the literature.[34,35] It is understood that since mass spectrometry involves gas-phase ions, care must be taken in using the fragmentation patterns observed in discussions of a heterogeneous thermal process such as CVD.[35] Nonetheless, our previous studies have shown that mass spectrometry of the tungsten imido precursors $Cl_4(CH_3CN)W(N^iPr)$ (**1a**) and $Cl_4(CH_3CN)W(NPh)$ (**2a**) affords qualitative insights into their CVD behavior.[28,30] We therefore use mass spectrometry of the precursor complexes as a preliminary screening technique to postulate possible fragmentation pathways before beginning CVD experiments. Results of a mass spectrometric study of the allylimido complex **3a** follow.

Table 1 summarizes the major fragment ions observed in the positive ion electron-impact (EI) and negative ion electron-capture chemical ionization (NCI) spectra of **3a**. As with the isopropyl and phenyl imido complexes **1a** and **2a**, no molecular ion was detected with either method. Instead, the highest mass envelopes in the EI and NCI spectra occurred at *m*/*z* 346 and 381, corresponding to $[Cl_3W(NC_3H_5)]^+$ and $[Cl_4W(NC_3H_5)]^-$ respectively. The $[Cl_3W(NC_3H_5)]^+$ fragment was also the base peak of the EI spectrum. A high abundance (95%) peak at *m*/*z* 41 corresponds to both acetonitrile ion $[CH_3CN]^+$ and loss of the allyl fragment $[C_3H_5]^+$ from the imido moiety.

Importantly, the base peak of the NCI spectrum corresponds to the mass envelope of the nitride fragment $[Cl_4WN]^-$ (*m*/*z* = 340). A small amount of the protonated nitrido complex fragment $[Cl_3WNH]^+$ was detected in the EI spectrum but at low relative abundance (∼12%). The observation of the nitride fragments $[Cl_3WNH]^+$ and $[Cl_4WN]^-$ indicates that the critical imido N−C bond is broken under ionization conditions. The lack of any molecular ion in either mass spectrum is consistent with the nitrile ligand being labile. As observed with precursors **1a** and **2a**, the EI spectrum of the allyl imido complex **3a** also exhibited fragments corresponding to loss of the imido nitrogen. Accordingly, mass envelopes at *m*/*z* 256 (27% abundance) and 291 (58% abundance) are assigned to the fragments $[Cl_2W]^+$ and $[Cl_3W]^+$, respectively.

Relative to the isopropyl and phenyl imido precursors **1a** and **2a**, the allyl complex **3a** shows some similarities and important differences. In each case, the base peak of the EI spectrum corresponds to the loss of $CH_3CN$ and one chloride ligand (i.e., $[Cl_3W(NR)]^+$). The abundance of the protonated nitrido fragment $[Cl_3WNH]^+$ in the EI spectrum of the allyl imido complex **3a** was only about 12% as compared to the 78% relative abundance of the same mass envelope in the spectrum of the isopropyl imido precursor **1a**. Strikingly, this fragment is not observed at all in the EI spectrum of the phenyl precursor. Additionally, the fragment corresponding to the loss of the nitrile ligand (i.e., $[Cl_4W(NR)]^-$) was observed in the NCI spectra of all three precursors. Interestingly, this fragment was the base peak for the NCI spectrum of the phenyl precursor **2a**. In contrast, the nitrido fragment $[Cl_4WN]^-$ was the base peak in the NCI spectra of the isopropyl and allyl complexes **1a** and **3a**, while this mass envelope only accounted for 4% relative abundance in the spectrum of **2a**. To the extent that the facile cleavages under mass spectrometric conditions are also facile under CVD conditions, one would expect higher nitrogen content in films from **1a** and **3a**.

The greater abundance of the nitrido fragment $[Cl_4WN]^-$ in the NCI spectra of **1a** and **3a** relative to **2a** indicates that the N−C bond of the imido ligand is more easily broken for the allyl and isopropyl imido precursors than for their phenyl imido analogue. This conclusion is supported by the absence of $[Cl_3WNH]^+$ in the EI spectrum of **2a** and its presence in the spectra of **1a** and **3a**. These data correlate well with the homolytic C−N bond dissociation energies reported for the corresponding amines (cf. $C_3H_5NH_2$ = 73 kcal/mol, $^iPrNH_2$ = 84 kcal/mol, and $PhNH_2$ = 105 kcal/mol).[36,37]

**X-ray Crystallographic Study of $Cl_4(CH_3CN)W(NC_3H_5)$ (3a).** The results of single-crystal structure determination of complex **3a** appear in Figure 1 and Tables 2 and 3. As has been

(34) Amato, C. C.; Hudson, J. B.; Interrante, L. V. *Mater. Res. Soc. Symp. Proc.* **1990**, *168*, 119−124.
(35) Lewkebandara, T. S.; Sheridan, P. H.; Heeg, M. J.; Rheingold, A. L.; Winter, C. H. *Inorg. Chem.* **1994**, *33*, 5879−5889.
(36) Benson, S. W. *Thermochemical Kinetics*, 2nd ed.; Wiley-Interscience: New York, 1976.
(37) Luo, Y.-R.; Holmes, J. L. *J. Phys. Chem.* **1994**, *98*, 303−312.

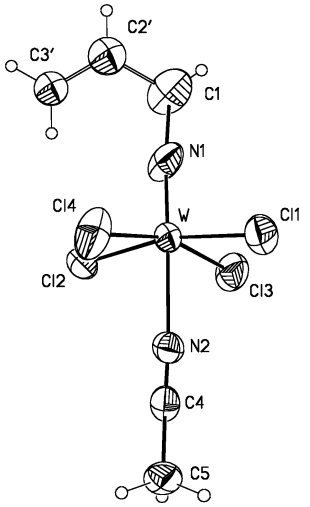


***Figure 1.*** Thermal ellipsoids diagram of the molecular structure of $Cl_4(CH_3CN)W(NC_3H_5)$ (**3a**). Thermal ellipsoids are plotted at 50% probability. The disordered carbon positions C(2) and C(3) of the allyl moiety are omitted for clarity.

***Table 2.*** Crystal Data and Structure Refinement for $Cl_4(CH_3CN)W(NC_3H_5)$ (**3a**)

| | | |
|---|---|---|
| empirical formula | $C_5H_8C_{l4}N_2W$ | |
| formula wt | 421.78 | |
| $T$ (K) | 173(2) | |
| wavelength (Å) | 0.71073 | |
| crystal system | monoclinic | |
| space group | $P2_1$ | |
| unit cell dimensions | $a = 6.1482(7)$ Å | $\alpha = 90°$ |
| | $b = 7.4742(8)$ Å | $\beta = 95.089(2)°$ |
| | $c = 12.3697(13)$ Å | $\gamma = 90°$ |
| volume (Å$^3$) | 566.18(11) | |
| Z | 2 | |
| density (calculated) (Mg/m$^3$) | 2.474 | |
| absorption coefficient (mm$^{-1}$) | 11.097 | |
| $F$(000) | 388 | |
| crystal size (mm$^3$) | 0.12 × 0.09 × 0.04 | |
| $\theta$ range for data collection (deg) | 1.65−27.50 | |
| index ranges | $-6 \le h \le 7$, $-8 \le k \le 9$, $-15 \le l \le 15$ | |
| reflections collected | 3692 | |
| ind reflections | 2287 [$R$(int) = 0.0442] | |
| completeness to $\theta = 27.50°$ | 98.6% | |
| absorption correction | integration | |
| max and min transmission | 0.6624 and 0.3050 | |
| refinement method | full-matrix least-squares on $F^2$ | |
| data/restraints/parameters | 2287/1/112 | |
| goodness-of-fit on $F^2$ | 1.047 | |
| final $R$ indices [$I > 2\sigma(I)$] | $R_1{}^a = 0.0372$, $wR_2{}^b =$ 0.0883 [1939] | |
| $R$ indices (all data) | $R_1 = 0.0469$, $wR_2 = 0.0936$ | |
| absolute structure parameter | 0.44(4) | |
| largest diff peak and hole (Å$^{-3}$) | 1.818 and −1.413 | |

[a] $R_1 = \sum(||F_o| - |F_c||)/\sum|F_o|$. [b] $wR_2 = [\sum[w(F_o^2 - F_c^2)^2]/\sum[w(F_o^2)^2]]^{1/2}$. $S = [\sum[w(F_o^2 - F_c^2)^2]/(n - p)]^{1/2}$. $w = 1/[\sigma^2(F_o^2) + (mp)^2 + np]$, $p = [\max(F_o^2,0) + 2F_c^2]/3$; $m$ and $n$ are constants.

previously reported for analogous tungsten imido complexes,[38,39] the overall geometry at the tungsten center is octahedral with the imido and acetonitrile ligands located in a trans orientation with respect to each other. The alkene carbons of the allyl moiety are disordered, and for brevity, only one set of positions [C(2)′ and C(3)′] will be discussed.

***Table 3.*** Selected Bond Distances (Å) and Angles (deg) for $Cl_4(CH_3CN)W(NC_3H_5)$ (**3a**)[a]

| | | | |
|---|---|---|---|
| W−N(1) | 1.687(9) | W−Cl(4) | 2.351(9) |
| W−N(2) | 2.308(8) | N(1)−C(1) | 1.508(17) |
| W−Cl(1) | 2.339(10) | C(1)−C(2)′ | 1.51(2) |
| W−Cl(2) | 2.317(8) | C(2)′−C(3)′ | 1.36(3) |
| W−Cl(3) | 2.324(9) | N(2)−C(4) | 1.130(12) |
| C(1)−N(1)−W | 167(2) | N(1)−W−N(2) | 175.8(15) |
| N(1)−W−Cl(2) | 90.6(8) | N(2)−W−Cl(2) | 86.0(7) |
| N(1)−W−Cl(3) | 93.6(7) | N(2)−W−Cl(3) | 84.0(6) |
| Cl(2)−W−Cl(3) | 88.7(4) | C(4)−N(2)−W | 175(3) |
| N(1)−W−Cl(1) | 102.4(8) | N(2)−W−Cl(1) | 81.1(7) |
| C(2)′−C(1)−N(1) | 114.2(21) | C(3)′−C(2)′−C(1) | 120(2) |
| Cl(3)−W−Cl(1) | 90.18(13) | N(2)−C(4)−C(5) | 178(2) |

[a] The structure of **3a** exhibits disorder in the carbon atoms C(2) and C(3) of the allyl moiety. Data for one set of olefinic carbon atoms [C(2)′ and C(3)′] are included. Data for the alternative set [C(2) and C(3)] can be found in the Supporting Information.

The W≡N bond length of the related chloroimido complex $Cl_4(CH_3CN)W(NCl)$ has been reported as 1.72(1) Å.[38] This value is somewhat longer than the W−N(1) distance of 1.687(9) Å observed for **3a**, reflecting the electronic differences in the chloroimido versus alkylimido ligands. The W≡N bond length of $Cl_4(THF)W(NC_6H_4CH_3$-$p)$[39] (1.711(7) Å) compares more favorably with that of **3a**, as expected for an alkylimido complex. The W−N distance for the nitrile ligand (2.28(1) Å) as well as the W−Cl bond lengths (2.350(3) and 2.316(3) Å) of $Cl_4(CH_3CN)W(NCl)$ are consistent with the analogous distances for **3a** and standard literature values.[40]

To our knowledge, there are no other reports of allylimido structures for tungsten; however, several molybdenum complexes containing the $NC_3H_5$ ligand have been reported, including the Mo(V) compound $Cl_3(OPPh_3)_2Mo(NC_3H_5)$.[41] Much like $Cl_3(OPPh_3)_2Mo(NC_3H_5)$, **3a** has a C(2)′−C(3)′ distance (1.36(3) Å) that is consistent with the presence of a double bond between these atoms. Furthermore, the C(3)′−C(2)′−C(1) angle of 120(2)° confirms the presence of sp$^2$ hybridized carbons at C(2) and C(3).

**Film Growth.** The low vapor pressure of the precursors made use of a solid-source delivery system impractical. To overcome this limitation, a nebulizer assembly was used to generate an aerosol of solvent/precursor droplets, which were delivered to the reactor by a heated impinging jet. After deposition was complete, the films typically had a smooth, shiny metallic surface, with colors ranging from gold to black, depending on deposition temperature.

**XRD of Films.** The X−ray diffraction (XRD) spectra in Figure 2 indicate amorphous and polycrystalline film deposition from complexes **3a**,**b** at 450 and 650 °C, respectively. The polycrystalline film has peak locations consistent with polycrystalline $\beta$-$WN_xC_y$. Four characteristic peaks are evident, indicating that no preferred crystal orientation was present in the films. Primary reflections at 37.18 and 43.33 $2\theta$° are consistent with (111) and (200) $\beta$-$WN_xC_y$ growth planes, while additional reflections at 62.88 and 74.88 $2\theta$° indicate (220) and (311) planes, respectively.

Figure 3 shows the evolution of film crystallinity with deposition temperature. For deposition at and below 525 °C, the characteristic $\beta$-$WN_x$ peaks are not observed. At 550 °C, a broad peak appears near 37.63 $2\theta$°, indicating polycrystalline

(38) Görge, A.; Dehnicke, K.; Fenske, D. *Z. Naturforsch., B: Chem. Sci.* **1988**, *43*, 677−681.
(39) Bradley, D. C.; Errington, R. J.; Hursthouse, M. B.; Short, R. L.; Ashcroft, B. R.; Clark, G. R.; Nielson, A. J.; Rickard, C. E. F. *J. Chem. Soc., Dalton Trans.* **1987**, 2067−2075.
(40) Orpen, A. G.; Brammer, L.; Allen, F. H.; Kennard, O.; Watson, D. G.; Taylor, R. *J. Chem. Soc., Dalton Trans.* **1989**, S1−S83.
(41) Du, Y. H.; Rheingold, A. L.; Maatta, E. A. *Inorg. Chem.* **1994**, *33*, 6415−6418.

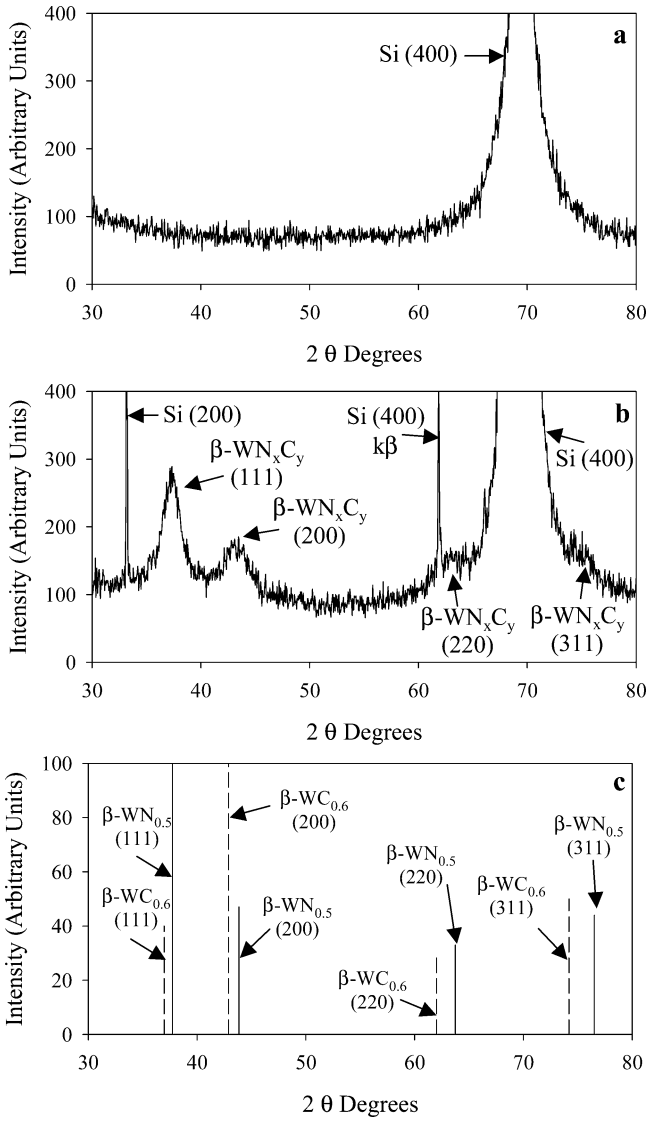


***Figure 2.*** XRD spectra for films grown with **3a**,**b** on Si (100) in a $H_2$ atmosphere. (a) 450 °C, (b) 650 °C, and (c) standard powder diffraction plots for $\beta$-$WN_{0.5}$ and $\beta$-$WC_{0.6}$.

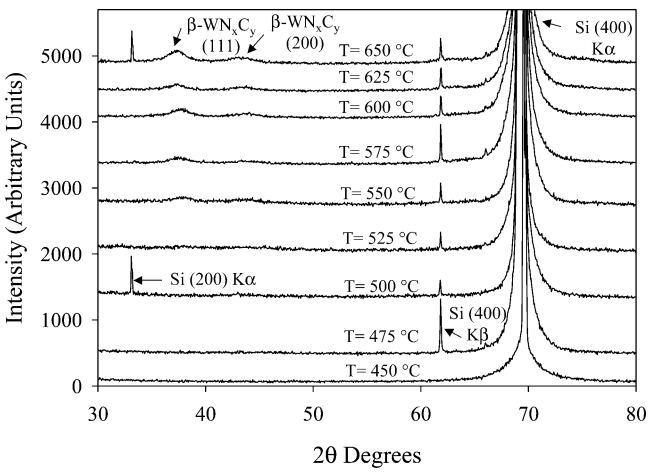


***Figure 3.*** Change in XRD pattern with deposition temperature for films grown from **3a**,**b** on Si (100) in a $H_2$ atmosphere.

$\beta$-$WN_xC_y$ (111) growth. As the deposition temperature increases to 575 °C, this peak sharpens, and a broad peak at 44.08 2$\theta$° appears, indicating $\beta$-$WN_xC_y$ (200) growth. The peaks sharpen further as the temperature approaches 650 °C, indicating polycrystalline grain growth. Some of the films displayed two additional peaks at 32.98 and 61.63 2$\theta$°, representing Si (200) K$\alpha$ and Si (400) K$\beta$ radiation, respectively. Broad peaks emerge at 63.33 and 75.43 2$\theta$° for growth at 650 °C, indicating $\beta$-$WN_xC_y$ (220) and (311) growth. Since the formation of polycrystalline films is highly undesirable for diffusion barrier applications, the ability to grow amorphous films by deposition with this precursor below 550 °C is significant.

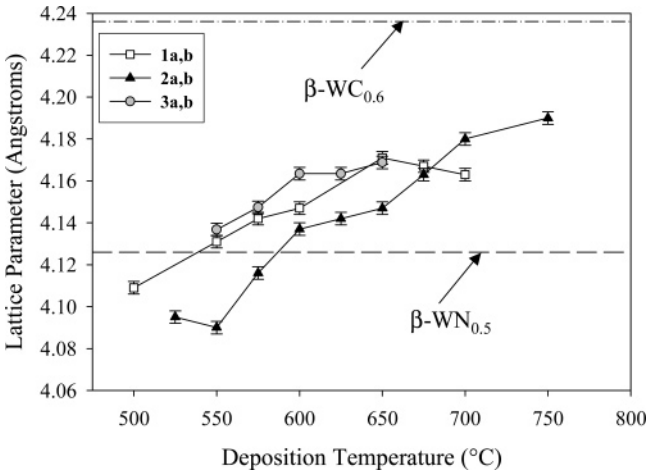


***Figure 4.*** Lattice parameters for films grown from **1a**,**b**, **2a**,**b**, and **3a**,**b** based on the $\beta$-$WN_xC_y$ (111) diffraction peak. The dashed line at 4.126 Å represents the standard lattice parameter value for $\beta$-$WN_{0.5}$, while the dash−dot line at 4.236 Å is that for $\beta$-$WC_{0.6}$. Error bars indicate uncertainty in the lattice parameter (±0.002 Å) due to X-ray K$\alpha$ line broadening.

The film crystallization for growth at 550 °C with **3a**,**b** can be compared to 500 and 525 °C for **1a**,**b** and **2a**,**b**, respectively. The maximum deposition temperature for films deposited from **3a**,**b** was 650 °C, as compared to 700 and 750 °C for **1a**,**b** and **2a**,**b**, respectively. For all three precursors, deposition above the respective maximum growth temperature resulted in formation of uncharacterized black particles on the substrate and susceptor, which subsequently compromised film quality.

**Lattice Parameter.** The dependence of the lattice parameter on deposition temperature in Figure 4 was determined by XRD using the 2$\theta$ position of the (111) $\beta$-$WN_xC_y$ diffraction peak, with peak position calibrated to the Si (400) diffraction peak. The standard $\beta$-$WN_{0.5}$ (111) and $\beta$-$WC_{0.6}$ (111) peak positions are 37.735 and 36.977 2$\theta$° (Figure 2c), respectively, and correspond to standard lattice parameter values of 4.126 and 4.236 Å. The position of the (111) reflection peak can vary as a result of a change in composition or a change in the film's residual stress. Since our films are highly disordered, especially when grown at lower temperatures, we assume that the strain is nonuniform and thus does not cause a shift in the center of the XRD peak.[42] Upon attributing compositional variation as responsible for the peak shift (and concomitant lattice parameter changes), trends in the relative concentrations of N, C, and Va (vacancies) in the interstitial sublattice can be suggested by coupling the peak shift with the compositions measured by AES, as discussed previously.[30] If the (111) peak position is higher than 37.735 2$\theta$°, corresponding to a lattice parameter below 4.126 Å, then minimal C, a deficiency of N, and an excess number of Va exist in the polycrystals. This condition is true

(42) Cullity, B. D. *Elements of X-ray Diffraction*; Addison-Wesley: Reading, MA, 1978.

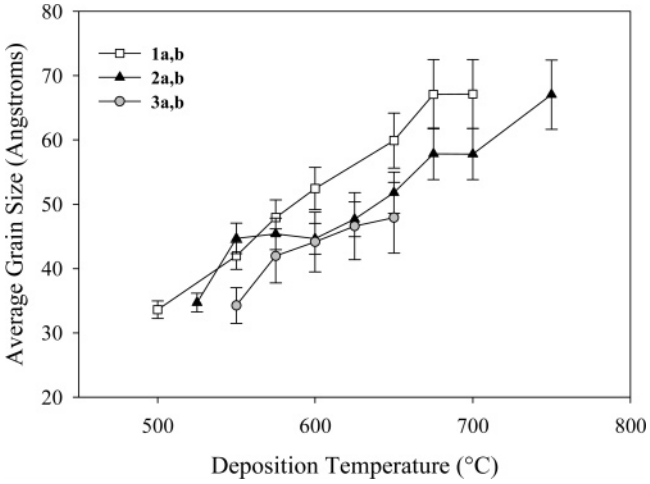


***Figure 5.*** Change in average grain size with deposition temperature for polycrystalline films grown from **1a**,**b**, **2a**,**b**, and **3a**,**b** based on the fwhm of the $\beta$-$WN_xC_y$(111) diffraction peak. Error bars reflect uncertainty in fwhm measurements.

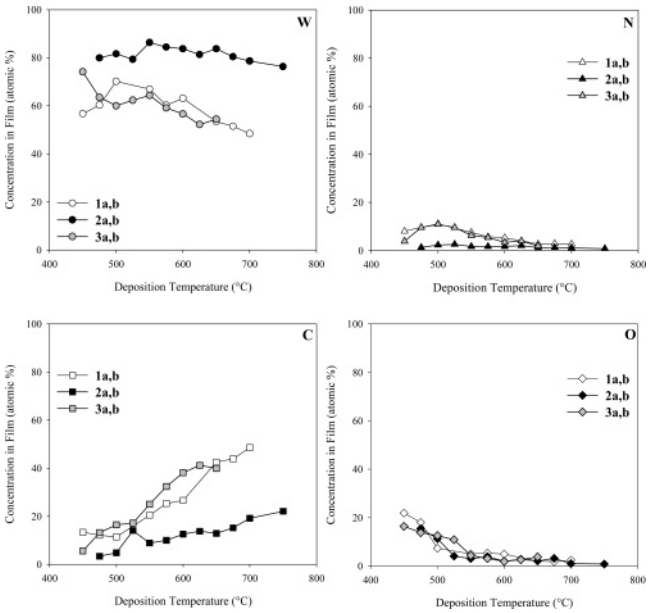


***Figure 6.*** Comparison of W, N, C, and O content in the films grown from **1a**,**b**, **2a**,**b**, and **3a**,**b**. Data are from AES measurements after 2.0 min sputter.

for deposition with **1a**,**b** at 500 °C. A peak position between 37.735 and 36.977 2$\theta$°, which corresponds to a lattice parameter between 4.126 and 4.236 Å, suggests mixing of N, C, and Va in the interstitial sublattice. This is the case for all polycrystalline films deposited from **3a**,**b**, and for films deposited at and above 550 °C with **1a**,**b**. As mentioned previously, however, $\beta$-$WN_xC_y$ polycrystals may form even at the lower temperatures, with C playing a role in the lattice parameter increase at lower temperatures.[30]

Values for the lattice parameter in the films grown from **3a**,**b** increase with deposition temperature. Between 550 and 600 °C, the lattice parameter increases from 4.14 to 4.16 Å. While N content decreases from 10 to 8 atom % through this temperature range, C content increases from 15 to 34 atom % (vide infra, Figure 6). An increase in lattice parameter coupled with constant or decreasing N levels, as occurs for films deposited above 550 °C, suggests that the amount of C incorporated into the interstitial sublattice is increasing in this region, causing expansion of the lattice. Increasing deposition temperature to 625 °C does not cause a change in lattice parameter; however, the lattice parameter does increase slightly for deposition at 650 °C to a maximum of 4.17 Å. This lattice parameter value coincides with the maximum lattice parameter for films deposited from **1a**,**b**, which also occurs at 650 °C.[28]

The lattice parameter was slightly higher for films deposited with **3a**,**b** relative to **1a**,**b** and was significantly higher than for **2a**,**b** at deposition temperatures $\leq$650 °C. Higher C content in films from **1a**,**b** and **3a**,**b** as compared to **2a**,**b** is consistent with lower lattice parameters for films from **2a**,**b** since less C is available to expand the polycrystalline lattice in films from **2a**,**b**. Since N levels are similar for polycrystalline films from **1a**,**b** and **3a**,**b**, differences in the lattice parameter are likely caused by differing C content on the interstitial sublattice. Interestingly, the lattice parameter for films deposited with both **1a**,**b** and **3a**,**b** is 4.17 Å at 650 °C. Accordingly, polycrystalline films deposited by **1a**,**b** and **3a**,**b** have adequate N, even at high temperatures, to be considered primarily $\beta$-$WN_x$ into which carbon is incorporated to form $\beta$-$WN_xC_y$. This is not the case for films from **2a**,**b**, however, that experience a shift toward $\beta$-$WC_y$ for deposition at temperatures above 675 °C.[30] The difference in lattice parameter for films from **1a**,**b** and **3a**,**b** at 450 °C suggests that the imido ligand plays a role in the deposition of C into the $\beta$-$WN_xC_y$ polycrystals.

**Polycrystal Grain Size.** Grain size ($t$) was estimated using the Scherrer equation.[28,42,43] The dominant (111) diffraction peak for the films was used as the reference peak for fwhm determination. As depicted in Figure 5, grain size for the films from **3a**,**b** increased with deposition temperature, varying from 34 to 48 Å over the 550−650 °C temperature range. Below 550 °C, the films were X-ray amorphous; hence, the maximum grain size for these films was below 34 Å. The grain size increases most rapidly between 550 and 575 °C, with grain growth slowing above this temperature. Increasing deposition temperature causes a competition between increased grain growth due to higher surface diffusivity and decreased grain growth due to increasing C concentration on the film surface (which inhibits surface diffusion). Interplay between these phenomena causes grain growth in regions with small shifts in carbon content and leveling off of grain size in regions with larger shifts in carbon content.

**Film Composition.** Auger results in Figure 6 indicate that W, N, C, and O were present in the films deposited from **3a**,**b**, while Cl was not detected. The lowest C level, 6 atom %, occurs at the lowest deposition temperature of 450 °C. The carbon content increases with deposition temperature from 6 to 38 atom % between 450 and 600 °C and then levels off. As in the case for films grown from **1a**,**b** and **2a**,**b**, the overall trend in C content for films grown from the allylimido complexes **3a**,**b** reflects the increasing tendency of the hydrocarbon groups present in the precursor ligands and the solvent to decompose with increasing deposition temperature.[31]

Carbon levels in the films from **3a**,**b** were slightly higher than those from **1a**,**b** for most deposition temperatures and significantly higher than those from **2a**,**b** (Figure 6). The fact that films from **2a**,**b** contained lower levels of both N and C than those from **1a**,**b** or **3a**,**b** suggests that the phenylimido moiety is more likely to dissociate intact than the isopropylimido

(43) Nagai, M.; Hirano, N.; Omi, S. *Jpn. J. Appl. Phys., Part 1* **2000**, *39*, 4558−4560.

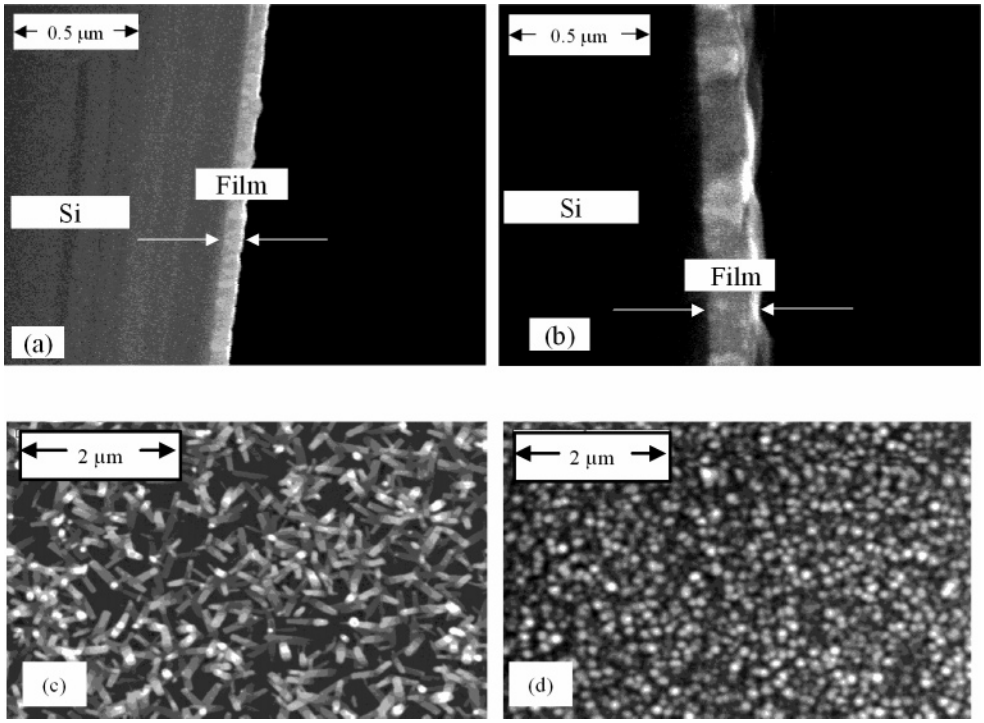


***Figure 7.*** SEM photos depicting films grown from **3a**,**b** on a Si (100) substrate: (a) cross-sectional view of film grown at 450 °C; (b) cross-sectional view of film grown at 650 °C; (c) morphology of film deposited at 450 °C; and (d) morphology of film deposited at 650 °C.

or allylimido fragments, consistent with the higher N−C bond strength in the phenylimido group.

The N content in films grown at 450 °C was 4 atom %, and this rose to a maximum of 11 atom % for deposition at 500 °C. Above 500 °C, the N levels decrease, dipping to 2 atom % at 650 °C. The higher N levels at lower temperature reflect the stability of the W−N multiple bond in the precursor molecule, which likely endures at deposition temperatures up to 500 °C, inhibiting release of N into the gas phase during deposition. The drop in N above 500 °C may indicate decomposition of the W−N multiple bond in the gas phase and/or increased N desorption from the film (to form $N_2$ gas) at higher temperatures.

Oxygen contamination resulted from post-growth exposure of the film samples to air, as demonstrated by incremental AES sputtering, which showed a steady decrease in O levels with increasing depth into the films. The O concentration was highest at 450 °C, reaching 16 atom %, and decreased slightly to 11 atom % at 525 °C. Amorphous films deposited below 550 °C had low density and high porosity, which allowed substantial amounts of oxygen to penetrate into the film lattice. As the deposition temperature was increased to 550 °C, the O content dropped sharply to 4 atom %. This observation is consistent with crystallization of the film in this temperature range. As the film crystallizes, its microstructure becomes denser, thereby inhibiting post-growth oxygen diffusion into the lattice.[7,44] As the deposition temperature increased above 550 °C, the O concentration dropped further, reaching a steady level near 3 atom % at the highest deposition temperatures. This resulted from further film densification (by polycrystal grain growth) and increased C levels at higher deposition temperature, which stuff the grain boundaries and block diffusion of oxygen into the films.

(44) Joseph, S.; Eizenberg, M.; Marcadal, C.; Chen, L. *J. Vac. Sci. Technol., B* **2002**, *20*, 1471−1475.

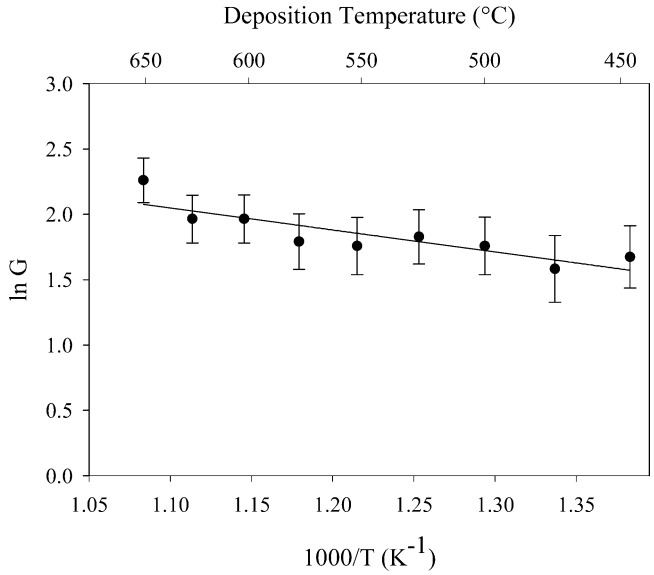


***Figure 8.*** Plot of film growth rate on Si (100) vs inverse temperature for deposition from **3a**,**b**. Error bars indicate uncertainty due to deposition temperature variation (±10 °C) and thickness measurement from XSEM photos.

**Film Growth Rate (XSEM).** Growth rates were estimated by dividing total film thickness (from X-SEM) by deposition time. Figure 7 depicts X-SEM photos for films grown at the lowest and highest growth temperatures (450 and 650 °C) that have deposition rates of 5 and 10 Å/min, respectively. An Arrhenius plot using the measured growth rates (Figure 8) indicates one growth regime, evidenced by a single line without any break points. The apparent activation energy ($E_a$) for deposition with **3a**,**b** was 0.15 eV, which is substantially lower than the typical activation energy range for CVD growth in the kinetic regime (0.5−1.0 eV).[45]

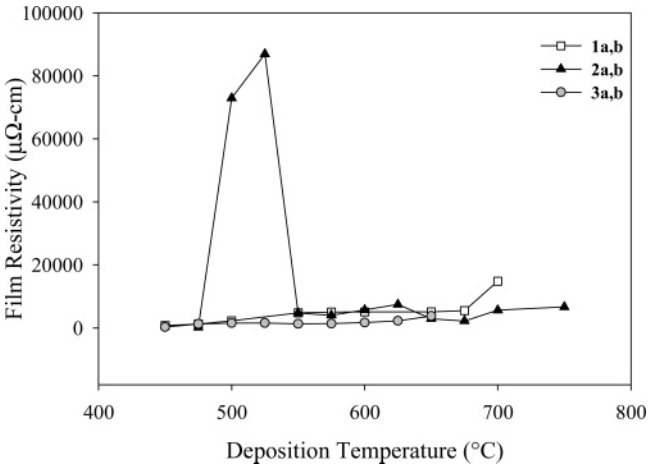


***Figure 9.*** Variation of film resistivity with deposition temperature for films deposited with **1a**,**b**, **2a**,**b**, and **3a**,**b**.

Deposition from **3a**,**b** at temperatures below 450 °C did not result in significant film growth. This result suggests that while cleavage of the N−C bond in the imido moiety may be an important propagation step for deposition from this family of precursors (vide infra), another gas phase or surface process likely dictates the minimum temperature required to initiate deposition on the substrate surface. Deposition at 675 °C resulted in deposition of black particles on the substrate and susceptor surface, indicating that gas-phase nucleation was occurring. For this reason, 650 °C was deemed to be the upper temperature limit for deposition from this precursor.

**Film Resistivity.** Film resistivity was calculated using eq 1

$$\rho = R_s t \tag{1}$$

where $\rho$ is resistivity (Ω cm), $R_s$ is sheet resistance (Ω/□) from a four-point probe measurement, and $t$ is film thickness (cm) from X-SEM. The variation of film resistivity with deposition temperature is shown in Figure 9. Deposition at 450 °C produced films with the lowest resistivity value (287 $\mu\Omega$ cm) despite C and O contamination levels of 6 and 16 atom %, respectively. This result is slightly higher than the 225 $\mu\Omega$ cm value for a film deposited at 475 °C with **2a**,**b** but lower than the 750 $\mu\Omega$ cm value observed for films grown at 450 °C from **1a**,**b**. The lower resistivity for films deposited at 450 °C from **3a**,**b** relative to **1a**,**b** was likely due to decreased N content in films from **3a**,**b**.

Film resistivity increases to 1260 $\mu\Omega$ cm for deposition with **3a**,**b** at 475 °C, likely due to increases in both N and C levels, which can increase film resistivity. The interplay of grain growth, carbon content, and film thickness causes the resistivity values to be steady up to 600 °C. Above this temperature, resistivity increases slightly, which is probably related to increased C content at higher temperature.

**Film Sheet Resistance.** To decouple the impact of film thickness from electrical properties, the sheet resistance was plotted as a function of deposition temperature (Figure 10). The sheet resistance results follow a similar trend as the film resistivity. The sheet resistance of films deposited from **3a**,**b** increases with deposition temperature from 36 Ω/□ at 450 °C to 172 Ω/□ at 475 °C and is fairly steady to 600 °C. Above 600 °C, the sheet resistance increases again, reaching a maximum value of 274 Ω/□ at 650 °C.

**Effect of the Imido N−C BDE on Film Growth.** In terms of their expected decomposition chemistry, the most significant difference between the isopropylimido complexes **1a**,**b**, the phenylimido complexes **2a**,**b**, and the allylimido complexes **3a**,**b** is the respective dissociation energies of the N−C bond in the imido ligand. Using the corresponding primary amines as organic model compounds, the N−C bond of complex **3a**,**b** should be approximately 11 kcal/mol weaker than the analogous bond in **1a**,**b** and 32 kcal/mol weaker than that in **2a**,**b**.[36] Since cleavage of this bond is necessary for deposition of $WN_x$, one would expect there to be differences in deposition behavior (Table 4) for the three precursors.

The $E_a$ for film deposition varied significantly for the three precursors, following a trend consistent with the strength of the imido N−C bond. Film deposition from **2a**,**b**, which possesses the strongest imido N−C bond, yielded the highest value for $E_a$ (1.41 eV), while that from **1a**,**b** yielded an intermediate value (0.84 eV). Deposition from **3a**,**b**, which has the weakest N−C bond, yielded the lowest $E_a$ (0.15 eV), which is well below the typical activation energy range for CVD growth in the kinetic regime (0.5−1 eV).[45] A plot of the $E_a$ values for deposition with the three precursors against the N−C bond strengths for the analogous amines is linear (Figure 11), with a goodness-of-fit ($R^2$) of 0.96. The linear relationship suggests that cleavage of the N−C imido bond is the rate-determining step in film growth from the **1a**,**b**, **2a**,**b**, and **3a**,**b** complexes. The strength of the bond in **3a**,**b** is so low, though, that film growth borders on being mass-transfer controlled. While the typical film growth temperature dependence[46] in the mass-transfer controlled region is $\sim T^{1.7-1.8}$, the temperature dependence for film growth from **3a**,**b** was slightly higher ($\sim T^{2.1}$), indicating that the rate-determining step for film growth from **3a**,**b** has a very weak kinetic barrier. Imido moieties with higher N−C bond energies, such as those in **1a**,**b** and **2a**,**b**, present a substantial kinetic constraint on film growth at lower temperature.

The strength of the N−C imido bond also has a strong effect on the amount of N incorporated into the film. If the N−C imido bond strength is relatively high, as with the phenylimido complexes **2a**,**b**, the imido group has a greater tendency to dissociate as an intact ligand via cleavage of the W−N bond, which leaves the films deficient in N. If the bond strength is relatively low, as with **1a**,**b** and **3a**,**b**, the alkyl group cleaves from the N more easily, leading to higher N levels in the film. It is interesting to note that unlike compounds **1a**,**b** and **2a**,**b**, allylimido complex **3a** gives conflicting information on the facility of N−C bond cleavage in its mass spectra. The $[Cl_4WN]^-$ ion is the base peak in the NCI spectrum of **3a**, while the ion corresponding to loss of the allyl moiety in the EI spectrum, $[Cl_3WNH]^+$, is present in only 12% abundance. Although the reason for this behavior is not clear, it may be an indicator of unanticipated difficulty in clean N−C cleavage under CVD conditions as well.

## Conclusions

Comparison of the film growth properties of **3a**,**b** to those of **1a**,**b** and **2a**,**b** allowed evaluation of the effect of the imido

(45) Raaijmakers, I. J.; Yang, J. *Appl. Surf. Sci.* **1993**, *73*, 31−41.

(46) Huang, M. Study of $TMGa-NH_3-N_2$ Systems Using in Situ Raman Spectroscopy. Ph.D. Dissertation, Department of Chemical Engineering, University of Florida, 2003.

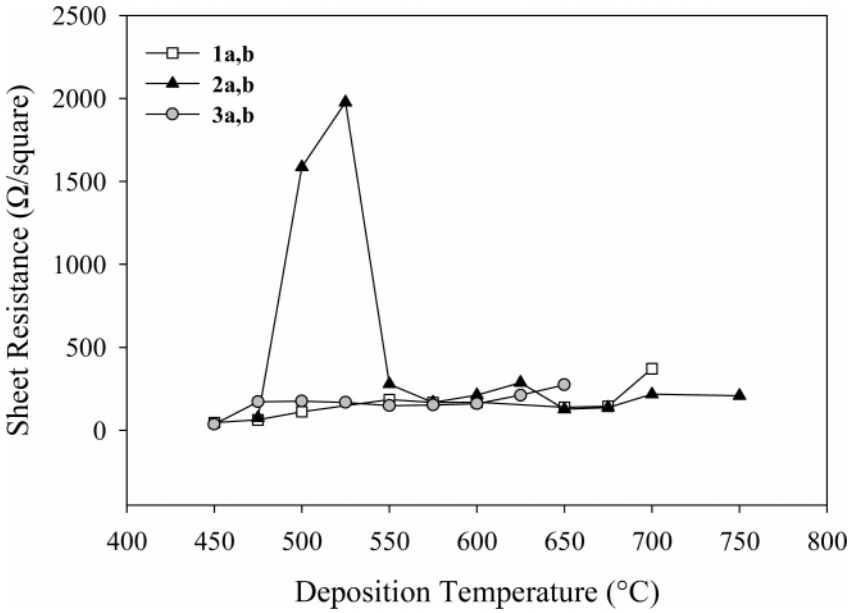


***Figure 10.*** Variation of sheet resistance with deposition temperature for films deposited from **1a**,**b**, **2a**,**b**, and **3a**,**b**.

***Table 4.*** Comparison of Deposition Behavior for **1a**,**b**−**3a**,**b**

| precursor | deposition temp. range (°C) | deposition rate (Å/ min) | $E_a$ (eV) | ref |
|---|---|---|---|---|
| $Cl_4(PhCN)W(NCH_2CH{=}CH_2)$ (**3a,b**) | 450−650 | 5−10 | 0.15 ± 0.13 | a |
| $Cl_4(PhCN)W(N^iPr)$ (**1a,b**) | 450−700 | 10−27 | 0.84 ± 0.23 | 27 |
| $Cl_4(PhCN)W(NPh)$ (**2a,b**) | 475−750 | 2−21 | 1.41 ± 0.28 | 29 |

[a] This paper.

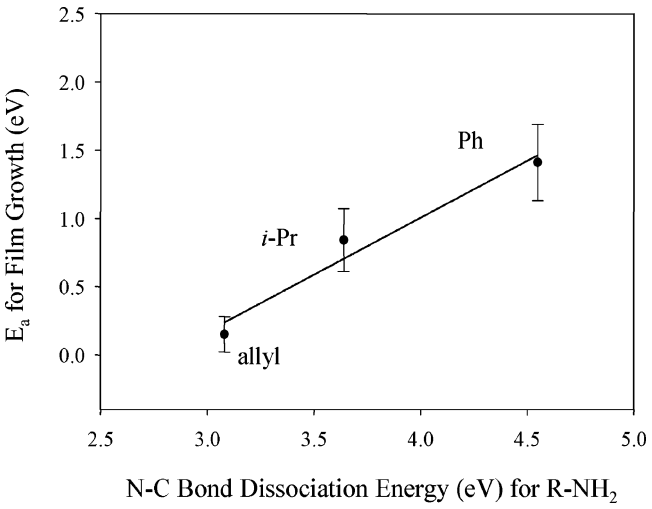


***Figure 11.*** Variation of apparent activation energy ($E_a$) for film growth from $Cl_4(R'CN)W(NR)$ (**1a**,**b**, R = $^i$Pr; **2a**,**b**, R = Ph; and **3a**,**b**, R = allyl) with the N−C bond energies of the corresponding amines R−$NH_2$ as models for the imido N−C bonds. Error bars reflect the uncertainty in film thickness measurement from XSEM images.

N−C bond dissociation energy on film growth and properties. Films deposited from **2a**,**b** were deficient in N as compared to those from **1a**,**b** and **3a**,**b**, consistent with a tendency of the stronger imido N−C bond of **2a**,**b** to result in dissociation of intact NPh fragments during deposition. Accordingly, an optimal window for N−C imido bond energy appears to exist in these precursors. If the energy of this bond is too high (as in **2a**,**b**), the W−N bond cleaves, leaving the films very deficient in N. If the bond energy is too low (as in **3a**,**b**), N−C bond cleavage may occur in the gas phase, leading to side reactions that consume the precursor before it reaches the substrate surface. A moderate N−C imido bond energy (as in **1a**,**b**) combines a substantial growth rate and better N retention during low-temperature growth with greater likelihood of N−C imido bond cleavage (relative to **2a**,**b**).

In practical terms, films grown from isopropylimido complexes **1a**,**b** are superior to those from phenylimido complexes **2a**,**b** for barrier applications because material produced from **1a**,**b** can be deposited at a lower minimum temperature (450 °C), contains more N, and has a lower sheet resistance.[30] Moreover, the isopropylimido precursor **1a**,**b** appears to be preferable to the allylimido precursor **3a**,**b**, due to higher growth rate and N content at their mutual lowest deposition temperature (450 °C). Design and synthesis of additional precursors based on the considerations discussed previously are underway.

**Acknowledgment.** We thank the National Science Foundation for support under NSF-CRC Grant CHE-0304810. K.A.A. wishes to acknowledge the National Science Foundation and the University of Florida for funding of the purchase of the single crystal X-ray equipment. Special thanks to Eric Lambers and Bradley Willenberg of the Major Analytical Instrumentation Center (MAIC) at the University of Florida for assistance with AES and X-SEM, respectively.

**Supporting Information Available:** Tables of bond distances, bond angles, positional parameters, and anisotropic displacement parameters for **3a**. This material is available free of charge via the Internet at http://pubs.acs.org.

JA043799D